Thermo-Elastic Characterization of Additively Manufactured Fiber Reinforced Composites

Yamuna H S [1], Manjula P H [2], Sangeetha S A [3]

[1] *Selection Grade Lecturer, Department of Chemical Engineering, S J (Government) Polytechnic Bengaluru, Karnataka, India.*

[2] *Selection Grade Lecturer, Department of Mechanical Engineering, Government Polytechnic Chintamani, Karnataka, India.*

[3] *Senior Scale Lecturer, Department of Ceramics Technology, S J (Government) Polytechnic Bengaluru, Karnataka, India.*

Abstract- This study uses physics to improve transfer learning and transfer the thermo-elastic properties of additively manufactured short fiber-reinforced polymers (SFRPs) between extrusion deposition additive manufacturing (EDAM) systems. Microstructural changes in similar materials printed on different machines change material characteristics, necessitating extensive testing for each new printer to enable exact process simulations. The suggested system reduces material characterisation needed to create digital material cards for additive process simulations. This is done by deducing the fiber and matrix's thermo-elastic properties using numerical data on printed system effectiveness. Inferred characteristics and microstructural descriptors are used to predict an alternate printing system's effectiveness. The fiber orientation tensor from the second system is mostly needed for the transfer procedure, decreasing characterization burden. The expected composite coefficient of thermal expansion (CTE) for the second printing system matches numerical values, proving the framework's capacity to convey information across systems. We also perform a sequentially linked thermo-mechanical study of two geometries in an EDAM simulation to investigate prediction errors. The transferred CTE values predict residual and spring-in deformations that match numerical CTE values, verifying the proposed approach's accuracy and efficacy.

Keywords: Fiber-reinforced polymers, Additive manufacturing, Thermo-elastic characterization.

1. INTRODUCTION

Short fiber-reinforced polymers (SFRPs) are popular because to their lightweight, low-cost manufacture, and design flexibility. Traditional manufacture involves injection molding discontinuous fiber-filled thermoplastic pellets. Extrusion deposition additive manufacturing (EDAM) has gained popularity for its capacity to create massive, complicated SFRP structures. The increased composite rigidity and lower CTE from fiber insertion increase scalability [1,2]. Large-scale EDAM has advanced significantly in the last decade. Oak Ridge National Laboratory built the first large-scale EDAM printer, Big Area Additive Manufacturing (BAAM), which can manufacture fiber-reinforced thermoplastics at 45 kg/hr. The Thermwood Corporation's Large Scale Additive Manufacturing (LSAM) technology, which prints and machines two pieces at 227 kg/hr, is another major achievement in large-scale EDAM printing. Purdue University introduced the Composite Additive Manufacturing Research Instrument (CAMRI), a mid-size EDAM printer for scientific research with production rates of 2–5 kg/hr. These machines introduce, melt, and extrude polymer ingredients loaded with fibers via a screw, depositing them on a construction platform according to machine-coded instructions. We recommend reading [3,4] to understand these printing systems' operations. The requirement for "first-time-right" printing is driven by the aerospace and automotive industries' rapid increase in applications, equipment, manufacturers, and models5. To achieve this, accurate and efficient simulation methodologies for production processes that account for form distortion in extrusion deposition additive manufacturing of SFRP components are needed. Cooling-induced shrinkage causes internal tensions and component deformation without external mechanical pressures. Material thermal expansion coefficients control thermomechanical shrinkage. Fibers aligned with the printing direction limit thermal expansion, resulting in a lower coefficient of thermal expansion (CTE) in that direction, while transversely where fiber reinforcement is less pronounced, shrinkage is greater. CTE must be characterized in all three spatial directions due to anisotropy. Printer-specific variances complicate matters. During printing, different printing processes create different material flow patterns, which change the microstructure and thermoelasticity of the material. Thus, every printer needs rigorous material characterization. Numerical characterisation is time-consuming and resource-intensive, and creating individual material cards for each machine limits additive manufacturing simulation technologies. This difficulty requires a robust information transmission mechanism amongst additive manufacturing technologies. This methodology would reduce numerical characterisation and speed process simulation. Knowledge transfer methods use insights from cheaper material and printer systems to improve the characterisation of more costly ones. Knowledge transfer approaches are popular in many fields, but their use in composite additive manufacturing is currently untested. A Bayesian transfer learning method was recently presented to estimate additively built SFRP thermal conductivity using tensile test microstructural features. This research introduces a micromechanics-based deterministic transfer learning paradigm for thermo-elastic characteristics in SFRP to address the absence of one.

2. CHARACTERIZATION OF THERMO-ELASTIC PROPERTIES

A research assessment of the material printed using the CAMRI system is the first step towards allowing the suggested knowledge transfer architecture. We employ an orthotropic description of the CTE to characterize the printed object. Measuring the CTE along the three main material directions—that of print direction (1-direction), in-plane direction transverse to the print direction (2-direction), and layer stacking direction (3-direction)—is thus necessary. This work uses 25% by weight carbon fiber (CF) Polyethersulfone (PESU) from Techmer (Electrafil PESU 1810 3DP). Following ASTM E83124 criteria, we describe the thermo-elastic qualities of SFRP materials. Starting with CTE sample preparation employing two different panel configurations—Panel A for measuring characteristics in 1-3 plane and Panel B for the 1-2 plane—as shown in Fig. 1, the procedure starts Comprising three beads printed across its width, Panel A (Fig. 1 (a) has final dimensions of 320 mm×18.45 mm×321mm (L×W×H). The printing settings listed in Table 1 guide the printing of the panels. Machined away after printing are the outside beads. Following removal of the top and bottom beads by machining, Panel B (Fig. 1 (b) has six beads in the 3-direction with final dimensions of 175 mm×159.9 mm×9mm (L×W×H).

TABLE 1 Printing parameters used during specimen fabrication

Parameter	Value
Nozzle Diameter	4 mm
Bead Width	6.15 mm
Bead Height	1.5 mm
Nozzle Area/Bead Area	1.44
Printing Speed	2540 mm/min

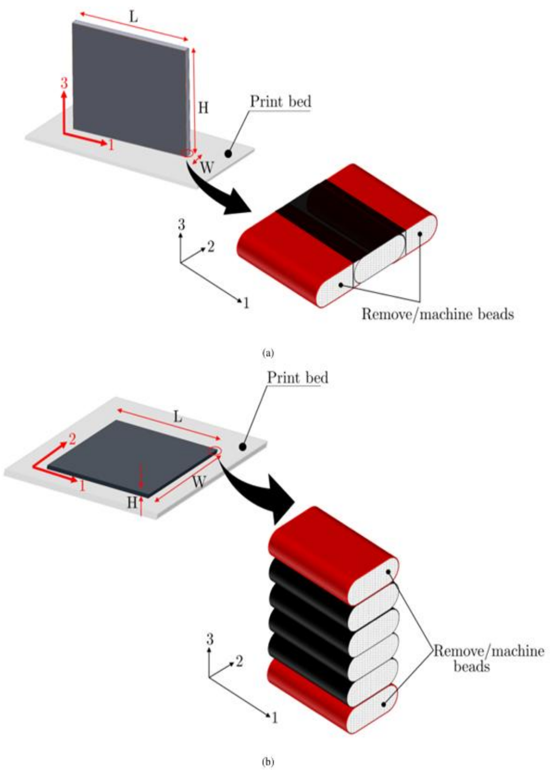

FIGURE 1. Schematic diagram of Panel A and B

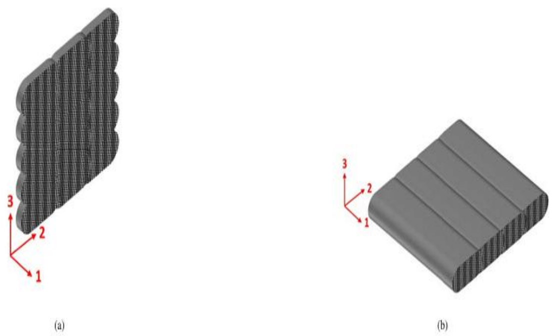

FIGURE 2. Schematic diagram of Specimen a and b

To reduce processing-induced residual stresses, we thermal annealed at a temperature somewhat below the polymer's glass transition temperature (Tg= 220◦C) after the printing and machining processes. With Panel B specimens planned to a thickness of 3 mm, the panels are then sectioned using a water jet to provide 25.4 mm × 25.4 mm square specimens (Fig. 2). We dry the specimens in an oven set at 100°C for two hours to eliminate moisture, therefore guaranteeing precise readings. Labeling, measuring cross-sectional areas, and putting a small layer of white speckles to one surface constitute the last preparatory procedures, therefore guaranteeing minimum coating to prevent interference with mechanical data. Following specimen preparation, we follow the CTE measuring process, which entails under a controlled temperature ramp measurements of the strain caused on the specimens. We precisely manage temperature fluctuations using an INSTEC Inc. precision thermal control tool. Every specimen is set on a Kapton sheet, which permits free thermal expansion and prevents molten material from adhesively attaching to the heating plate. Digital image correlation (DIC) records strain during heat cycling. Perfectly aligned with the sample plane, a digital camera is positioned above the sample to maximize capturing the whole speckle-patterned surface. Then, by varying aperture, focus, and exposure, the single-camera DIC system is calibrated. Images are captured at 5-second intervals throughout the thermal cycle while the specimen experiences a regulated temperature profile: heating to 350°C at 2°C/min, sustaining this temperature for 15 minutes, then cooling to room temperature at 2°C/min.

3. MICRO-MECHANICALPREDICTION OF THERMO-ELASTIC PROPERTIES

Our suggested system revolves around a micromechanics model at its heart. Once the component CTEs of the polymer and fibers are deduced, we forecast the CTE of the composite using the micromechanics model with a different microstructure. CTEs for SFRP materials generated in both CAMRI and LSAM systems may therefore be predicted using this calibrated micromechanics model. Among many techniques for assessing fiber-reinforced composite qualities, micromechanics-based methods—especially Eshelby based mean-field homogenization (MFH)—offer an effective means to assess the link between microstructure and bulk properties. Approximate stress and strain field averages at both the representative volume element (RVE) and individual phase levels are obtained via MFH methods. Although simpler MFH methods exist—e.g., the Reuss model (assuming uniform stress)—these are insufficient for our material system because of its naturally non-uniform fields. Rather, we use the more sophisticated Mori-Tanaka technique, which has shown efficacy in forecasting two-phase composite properties, especially for materials with a low fiber concentration (around 25% by weight for carbon fibers). Comprising a thermoplastic polymer reinforced with small carbon fibers, our material system shows different fiber orientation and length distributions.

Two main stages define the homogeneity process: Each homogenized using the Mori-Tanaka model replaces the real composite RVE with a model consisting pseudo-grain aggregates with inclusions of the same orientation state and length; then, using the Voigt model, find the effective response of these homogenized pseudo-grains. We use the Digimat program using inputs including fiber orientation, fiber aspect ratio, polymer matrix parameters, and transversely isotropic fiber properties. From the current literature, the fiber orientation tensor matching the CAMRI system and the characteristics of the component fibers and the matrix of this material were derived. By use of a micromechanics model calibration method, the component fiber and matrix CTEs are derived from the numerically observed CTEs from the CAMRIsystem.

4. RESULTS AND DISCUSSION

Fig. 3 shows the actual thermal strain against temperature data derived for the CAMRI system-printed specimens. Table 2 summarizes the measured CTE values—derived from the slopes of these strain-temperature curves by linear regression.

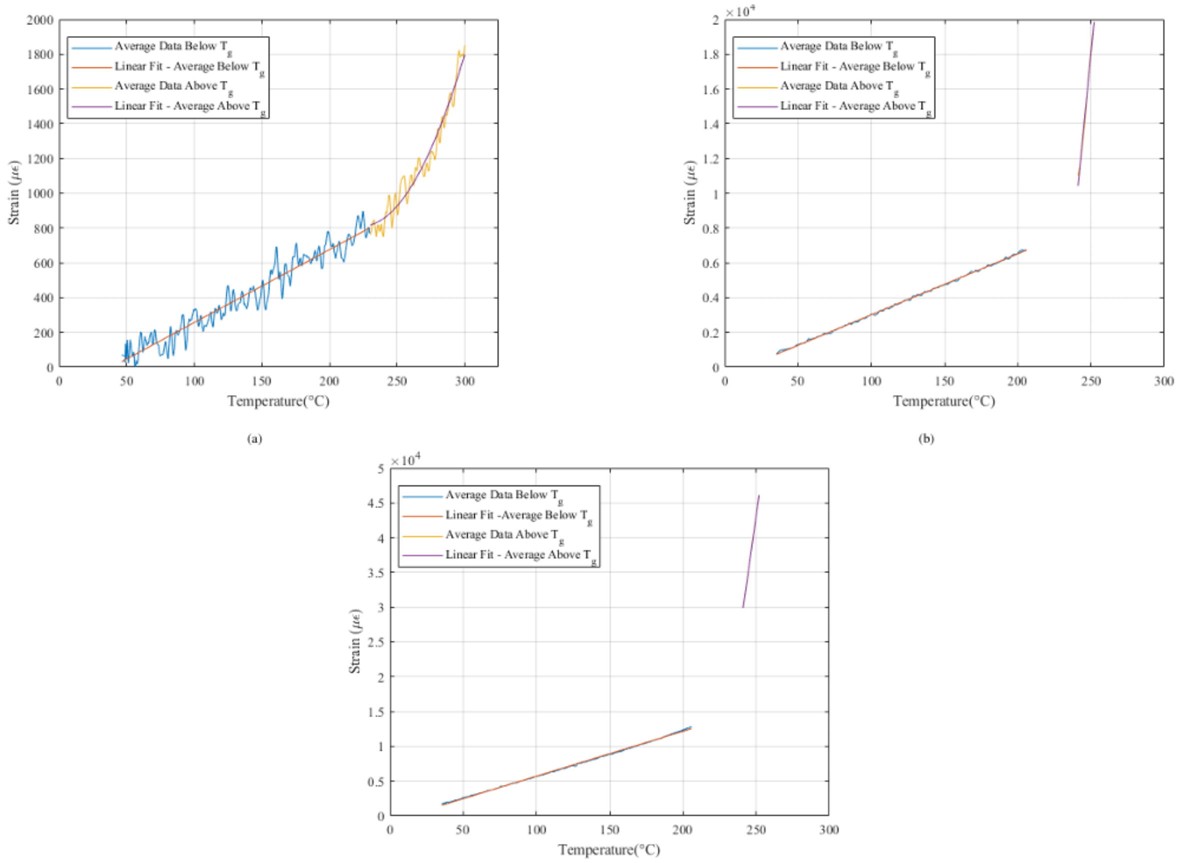

FIGURE 3. Strain vs temperature data obtained from CAMRI system in (a) 1 direction, (b) 2 direction, and in (c) 3 direction

TABLE 2 Researcher observed CTE values for the CF-PESU material printed in CAMRI

α^1_{exp} (μ ε/°C)	α^2_{exp} (μ ε/°C)	α^3_{exp} (μ ε/°C)
4.19	35.08	64.52

We address the component property inference issue using these CAMRI system Researcher data. Tables 3–5 show the fiber and matrix parameters derived from literature, which provided micromechanics model inputs. Table 6 lists the inferred component CTE values produced by the optimizing procedure. While polysulfone-based polymers usually have CTEs ranging from 54.7 to 56.9μ λ, these findings fit well with existing literature values where carbon fiber usually shows CTEs between-1.36 and-0.36 μ λ in the fiber direction and 8 to 18 μ λ in the transverse direction.

TABLE 3 Material properties of constituent carbon fiber

E_{11} (N/mm^2)	$E_{22} = E_{33}$ (N/mm^2)	G_{23} (N/mm^2)	$\nu_{12} = \nu_{13}$	ν_{23}	aspect ratio	mass fraction	density (kg/m^3)
2.40×10^5	1.4×10^4	2.8×10^4	0.2	0.25	20	0.25	1800

TABLE 4 Material properties of constituent matrix

E (N/mm^2)	ν	density (kg/m^3)
2.34×10^3	0.343	1350

TABLE 5 Fiber orientation tensor for CAMRI system

a_{11}	a_{22}	a_{33}
0.771	0.163	0.066

TABLE 6 Inferred CTE values for the fiber and matrix material of CF-PESU Part printed in CAMRI

α^1_f (μ ε/°C)	α^2_f (μ ε/°C)	α_m (μ ε/°C)
-1.25	12.2	56.09

TABLE 7 Micromechanically predicted CTE values for the CF-PESU material printed in CAMRI

α^1_{pred} (μ ε/°C)	α^2_{pred} (μ ε/°C)	α^3_{pred} (μ ε/°C)
4.19	37.59	59.34

TABLE 8 Micromechanically predicted CTE values for the SFRP system printed in LSAM

α^1_{pred} (μ ε/°C)	α^2_{pred} (μ ε/°C)	α^3_{pred} (μ ε/°C)
8.19	26.08	53.3

TABLE 9 Researcher observed CTE values for the SFRP system printed in LSAM

α^1_{exp} (μ ε/°C)	α^2_{exp} (μ ε/°C)	α^3_{exp} (μ ε/°C)
8.7	28.16	63.7

First, using the estimated component CTE characteristics, we forecast the composite CTE values for the CAMRI system (Table 7), thereby verifying that we estimate the relevant constituent CTE properties. With variances of 0.00%, 7.16%, and 8.03% in the 1-, 2-, and 3-directions correspondingly, all within a reasonable 10% error range, a comparison with Researcher data demonstrated outstanding agreement. We then anticipate the CTE values, for the same material, but produced using the LSAM technique, hence illustrating knowledge transfer across printing technologies. Maintaining all other material characteristics unaltered, this approach needed just simple tensile testing to find the orientation tensor of the LSAM system (Table 7). The technique described helps one to get the fiber orientation. Table 8 lists the expected CTE values for the LSAM system. We performed numerical measurements (Table 9) and a comparison revealed acceptable agreement with errors of 5.86%, 7.39%, and 16.33% in the 1-, 2-, and 3-directions, respectively, thereby evaluating the correctness of the expected CTEs of the material produced in the LSAM system.

5. CONCLUSIONS

This paper presents a framework for transferring the thermo-elastic properties of short fiber-reinforced polymers (SFRPs) across different extrusion-based additive manufacturing methods. This technology significantly minimizes the extensive material characterization often required to develop virtual twins of SFRP production processes. The following steps comprise our proposed framework: Initially, using a 25% carbon fiber-reinforced PESU composite fabricated with CAMRI technology, we deduced the component fiber and matrix coefficients of thermal expansion (CTEs) utilizing Powell's method, a gradient-free local optimization technique. The inferred values for this material system aligned well with the anticipated ranges. By using these deduced component values, we successfully predicted the CTEs of the composite, so validating both our framework and the foundational micromechanical model.

Subsequently, using the component characteristics derived from the CAMRI system, we used this framework to predict CTEs for the same material composition fabricated using an alternative approach (LSAM). The only numerical characterisation necessary for the LSAM system was a simple tensile test to determine the fiber orientation tensor. The numerical measurements and the anticipated CTE values exhibited strong concordance, suggesting that the characteristics were effectively conveyed via the printing procedures. We conducted simulations of two test cases—a flat plate and a racetrack configuration produced using the LSAM system—to further validate our methodologies. The racetrack shape exhibited an 8.2% disparity in spring-in deformation between the two value sets, but the flat plate had comparable mid-plane deformations regardless of whether predicted or numerical CTEs were used. These results confirm the accuracy and relevance of our paradigm in practical situations.

Given these promising results, we want to explore the extension of this paradigm in further research to transfer thermo-visco-elastic properties to other printing techniques. Moreover, one may examine the impact of varying fiber orientations within a printed component on the assessment of thermo-elastic properties, rather than depending on a singular average orientation. The proposed design may provide benefits for many additive manufacturing platforms, enhancing its applicability beyond the printing systems discussed below.

REFERENCES

[1] LoveL, KuncV, RiosO,etal. The importance of carbon fiber to polymer additive manufacturing. Journal of Materials Research. 2014;29(17):1893 1898.

[2] Thomas A, Jaszczuk M, Barocio E, Ghosh G, Bilionis I, Pipes RB. Probabilistic physics-guided transfer learning for material property prediction in extrusion deposition additive manufacturing. Computer Methods in Applied Mechanics and Engineering. 2014 ;419:116660.

[3] Brenken B. Extrusion Deposition Additive Manufacturing of Fiber Reinforced Semi-Crystalline Polymers. PhD thesis. Purdue University, West Lafayette, IN, USA; 2017.

[4] Barocio E. Fusion Bonding of Fiber Reinforced Semi-Crystalline Polymers in Extrusion Deposition Additive Manufacturing. PhD thesis. Purdue University, West Lafayette, IN, USA; 2020.

[5] Yakout M, Elbestawi M. Additive manufacturing of composite materials: an overview. In: Polytechnique Montreal, Canada. 2017; Montreal, Canada.

[6] Mortazavian S, Fatemi A. Effects of fiber orientation and anisotropy on tensile strength and elastic modulus of short fiber reinforced polymer composites. Composites Part B: Engineering. 2015;72:116–129.

[7] Compton B, Post B, Duty C, Love L, Kunc V. Thermal analysis of additive manufacturing of large-scale thermoplastic polymer composites. Additive Manufacturing. 2017;17:77–86.

[8] Brenken B, Barocio E, Favaloro A, Kunc V, Pipes RB. Development and validation of extrusion deposition additive manufacturing process simulations. Additive Manufacturing. 2019;25:218–226.

[9] Pibulchinda P, Barocio E, Pipes RB. Influence of Fiber Orientation on Deformation of Additive Manufactured Composites. Additive Manufacturing. 2021:102483.

[10] Barocio E, Pibulchinda P, Thomas A, Kapre V, Franc A. Validated Simulation for Large Scale Additive Manufacturing. CAMX 2022. 2022.

[11] Mori T, Tanaka K. Average stress in matrix and average elastic energy of materials with misfitting inclusions. Acta Metallurgica. 1973;21(5):571 574.

[12] Schapery R. Thermal expansion coefficients of composite materials based on energy principles. Journal of Composite Materials. 1968;2(3):380–404.

[13] Rosen BW, Hashin Z. Effective thermal expansion coefficients and specific heats of composite materials. International Journal of Engineering Science. 1970;8(2):157–173.

[14] Sideridis E. Thermal expansion coefficients of fiber composites defined by the concept of the interphase. Composites Science and Technology. 1994;51(3):301–317.

[15] Shen Y. Thermal expansion of metal–ceramic composites: a three-dimensional analysis. Materials Science and Engineering: A. 1998;252(2):269 275.

[16] Islam R, Sjölind S, Pramila A. Finite element analysis of linear thermal expansion coefficients of unidirectional cracked composites. Journal of Composite Materials. 2001;35(19):1762–1776.

[17] Aghdam M, Dezhsetan A. Micromechanics based analysis of randomly distributed fiber reinforced composites using simplified unit cell model. Composite Structures. 2005;71(3-4):327–332.

[18] Karadeniz ZH, Kumlutas D. A numerical study on the coefficients of thermal expansion of fiber reinforced composite materials. Composite Structures. 2007;78(1):1–10.

[19] Pan J, Bian L. Coefficients of nonlinear thermal expansion for fiber-reinforced composites. Acta Mechanica. 2017;228(12):4341–4351.

[20] Eshelby J. The determination of the elastic field of an ellipsoidal inclusion, and related problems. Proceedings of the Royal Society of London. Series A. Mathematical and Physical Sciences. 1957;241(1226):376–396.